J. Fluid Mech. (1986), *vol.* 164, *pp.* 469–485
Printed in Great Britain

Oscillatory instabilities of convection rolls at intermediate Prandtl numbers

By E. W. BOLTON, F. H. BUSSE AND R. M. CLEVER

Department of Earth and Space Sciences and Institute of Geophysics and Planetary Physics, University of California at Los Angeles, Los Angeles, CA 90024, USA

(Received 6 May 1985 and in revised form 14 October 1985)

The analysis of the instabilities of convection rolls in a fluid layer heated from below with no-slip boundaries exhibits a close competition between various oscillatory modes in the range $2 \lesssim P \lesssim 12$ of the Prandtl number P. In addition to the even-oscillatory instability known from earlier work two new instabilities have been found, each of which is responsible for a small section of the stability boundary of steady rolls. The most interesting property of the new instabilities is their close relationship to the hot-blob oscillations known from experimental studies of convection. In the lower half of the Prandtl-number range considered the BO2-mode dominates, which is characterized by two blobs each of slightly hotter and colder fluid circulating around in the convection roll in a spatially and time-periodic fashion. At higher Prandtl numbers the BE1-mode dominates, which possesses one hot blob (and one cold blob) circulating with the convection velocity. Just outside the stability boundary there exist other growing modes exhibiting three or four blobs which may be observable in experiments.

1. Introduction

The onset of oscillations in convection flows has received much attention in the literature since it is often viewed as a major step in the evolution of turbulence in fluid layers heated from below. Oscillations do indeed precede the transition to chaos in small convection boxes (Gollub & Benson 1980) or when the convection rolls are constrained by a magnetic field (Fauve, Laroche & Libchaber 1981). In large-aspect-ratio layers, on the other hand, a direct transition to aperiodic motions takes place, which appears to be induced by the skewed-varicose instability (Ahlers & Behringer 1978; Gollub & Steinman 1981). Even in the latter case the onset of oscillations can be noticed at higher Rayleigh numbers in the form of peaks above a broad frequency spectrum.

Much of the experimental work in recent years has focused on fluids with Prandtl numbers P in the range $2 \lesssim P \lesssim 7$ in order to demonstrate the interesting phenomena associated with low-Prandtl-number fluids. Liquid metals, liquid helium and gases have lower Prandtl numbers, but do not easily offer the opportunities for visualization of fluid motions that are available for transparent liquids such as water. Water is a particularly suitable liquid since its Prandtl number changes from a value of about 7 at room temperature to a value of less than 2 near its boiling point. The increasing number of experiments carried out in this intermediate range of Prandtl numbers has motivated the authors of this paper to extend the earlier work on the instabilities of convection rolls to this domain of the parameter space. In the papers by Clever & Busse (1974) and Busse & Clever (1979) the attention has been focused on the cases

$P = 7$ and $P = 0.71$ and the belief was expressed that only quantitative changes of the stability boundaries are to be expected between these two Prandtl numbers. The computations turned out to be especially costly in that range of Prandtl numbers and the stability boundaries were calculated only for a few discrete values of the wavenumber α of the convection rolls, as a function of the Prandtl number, throughout this regime. The new computations reported in this paper confirm the expectations based on the older work for the major part of the stability boundary of convection rolls in the (R, α)-space. The picture is changed, however, at the high-Rayleigh-number portion of the stability boundaries because of the appearance of new modes of oscillatory instability. These modes are characterized by the circulation of blobs of fluids which are hotter or colder than the time average at the respective position of the fluid layer. Oscillations of this kind have long been known from experimental observations of convection (Krishnamurti 1970; Busse & Whitehead 1974), even though they are usually not observed as instabilities of rolls. As in the case of other mechanisms of instabilities, the oscillatory blob instabilities are relatively little modified when they are preceded by another transition from rolls to three-dimensional forms of convection. The theoretical analysis presented in this paper thus has a more general range of application than is evident from the mathematical formulation.

The analysis starts in §2 with a brief outline of the mathematical methods. For a detailed description of the equations the reader is referred to earlier work, where the same methods have been used. In §3 an overview of the instabilities is given and a classification based on their symmetry properties is outlined. The stability boundaries for the Prandtl numbers 2.5 and 4.0, are described in §4 and the two-blob instability is discussed in some detail. The stability boundaries at higher Prandtl number are discussed in §5, where the one-blob instability is also described. In order to complete the description of the stability boundaries in the parameter space, cross-sections are presented for given values of the Rayleigh number R and of the wavenumber α in §6. The paper closes with a general discussion of the results in relationship to experimental observations and other theoretical work.

2. Outline of the mathematical methods

We consider a horizontal fluid layer heated from below with upper and lower rigid boundaries which are kept at the temperatures T_1 and T_2 respectively. The dimensionless Navier–Stokes equations in the Overbeck–Boussinesq approximation and the heat equation are given by equations (1), (2) and (3) of Clever & Busse (1984), hereinafter referred to as I. The height d of the layer, d^2/κ and $(T_2 - T_1)/R$ are used as scales for length, time and temperature respectively, where κ denotes the thermal diffusivity and R is the Rayleigh number. The velocity field $\boldsymbol{v}$ is described in terms of a general representation for a solenoidal vector field

$$\boldsymbol{v} = \nabla \times (\nabla \times \lambda\phi) + \nabla \times \lambda\psi,$$

where λ is the vertical unit vector. By taking the vertical components of the curl and the curl (curl) of the equation of motion two equations for the functions ψ and ϕ are obtained. The third equation of the problem is the heat equation for the deviation θ of the temperature from its static distribution. These equations are given by (5), (6), and (7) of I and must be solved subject to the boundary conditions

$$\phi = \frac{\partial}{\partial z}\phi = \psi = \theta = 0 \quad \text{at } z = \pm\tfrac{1}{2}, \tag{2.1}$$

where a Cartesian system of coordinates has been used with the z-coordinate in the vertical direction.

The analysis proceeds in two steps. First, two-dimensional steady nonlinear solutions are obtained which describe the convection rolls observed in experiments. In the second step infinitesimal disturbances of arbitrary three-dimensional form are superimposed onto the steady solution. If a growing disturbance is found, the roll solution is unstable; if no growing infinitesimal disturbance exists, the steady solution is regarded as stable. Since steady roll solutions exist as a function of R, P and α, a complete stability analysis requires the investigation of a three-dimensional parameter space of steady solutions. Fortunately, since the stability properties depend sufficiently smoothly on the parameters in general, costly detailed computations are required only in special cases.

The steady solution is obtained by a Galerkin technique. Since ψ vanishes for the two-dimensional case, only ϕ and θ have to be expanded in terms of orthogonal functions satisfying the respective boundary conditions,

$$\left.\begin{aligned}\phi &= \sum_{\lambda,\nu} a_{\lambda\nu}\, \mathrm{e}^{\mathrm{i}\lambda\alpha y} g_\nu(z) \equiv \sum_{\lambda,\nu} a_{\lambda\nu}\phi_{\lambda\nu},\\ \theta &= \sum_{\lambda,\nu} b_{\lambda\nu}\, \mathrm{e}^{\mathrm{i}\lambda\alpha y} f_\nu(z) \equiv \sum_{\lambda\nu} b_{\lambda\nu}\theta_{\lambda\nu}.\end{aligned}\right\} \tag{2.2}$$

Explicit expressions for $g_\nu(z)$ and $f_\nu(z)$ are given in I. The summation runs through all integers $1 \leqslant \nu \leqslant N$, $-N+\nu \leqslant \lambda \leqslant N-\nu$, where the truncation parameter N is chosen such that the solution changes by a negligible amount when N is replaced by $N+2$. The basic equations admit a subset of solutions of the form (2.2) which is characterized by the symmetry with respect to $y = 0$ and by the following symmetry with respect to the axis of the convection roll:

$$\phi(y, z) = -\phi\left(\frac{\pi}{\alpha} - y, -z\right), \quad \theta(y, z) = -\theta\left(\frac{\pi}{\alpha} - y, -z\right). \tag{2.3}$$

The symmetry in y implies that all coefficients $a_{\lambda\nu}$, $b_{\lambda\nu}$ are real with $a_{-\lambda\nu} = a_{\lambda\nu}$, $b_{-\lambda\nu} = b_{\lambda\nu}$, while condition (2.3) requires that all coefficients with odd $\lambda+\nu$ vanish. Since only convection rolls described by this subset of solutions have been observed, solutions outside the subset will not be considered.

As in I we use the following general description for the three-dimensional infinitesimal disturbances:

$$\left.\begin{aligned}\tilde{\phi} &= \{\sum_{\lambda,\nu} \tilde{a}_{\lambda\nu}\, \mathrm{e}^{\mathrm{i}\lambda\alpha y}\, g_\nu(z)\}\, \mathrm{e}^{\mathrm{i}(dy+bx)+\sigma t},\\ \tilde{\psi} &= \{\sum_{\lambda,\nu} \tilde{c}_{\lambda\nu}\, \mathrm{e}^{\mathrm{i}\lambda\alpha y}\, f_\nu(z)\}\, \mathrm{e}^{\mathrm{i}(dy+bx)+\sigma t},\\ \tilde{\theta} &= \{\sum_{\lambda,\nu} \tilde{b}_{\lambda\nu}\, \mathrm{e}^{\mathrm{i}\lambda\alpha y}\, f_\nu(z)\}\, \mathrm{e}^{\mathrm{i}(dy+bx)+\sigma t}.\end{aligned}\right\} \tag{2.4}$$

Substitution of (2.4) in the stability equations leads to a system of linear homogeneous equations for the coefficients $\tilde{a}_{\lambda\nu}$, $\tilde{b}_{\lambda\nu}$, $\tilde{c}_{\lambda\nu}$ with σ as the eigenvalue. The eigenvalue σ with the maximum real part $\sigma_{\mathrm{r\,max}}$ is determined as a function of b and d. This computation is repeated for several values of R and α, which are chosen such that they straddle the line in the (R, α)-plane on which $\sigma_{\mathrm{r\,max}}$ vanishes. If the values of R and α at which $\sigma_{\mathrm{r\,max}}$ has been calculated are sufficiently close, the stability boundary $\sigma_{\mathrm{r\,max}} = 0$ can be determined by interpolation. This method has been

successfully employed in I and in several other papers. The inaccuracies introduced by the interpolation are usually negligible in comparison with those caused by a finite value of the truncation parameter N.

3. Instabilities of convection rolls

The relatively high symmetry of the steady roll solution permits the separation of disturbances of the form (2.4) into several subsets. Because of the symmetry (2.3) the solutions of the stability equations have vanishing coefficients $\tilde{a}_{\lambda\nu}$, $\tilde{b}_{\lambda\nu}$ either for odd or for even $\lambda+\nu$. In table 1 these cases correspond to odd and even reflection or R-symmetry respectively. The coefficients $\tilde{c}_{\lambda\nu}$ in the expansion of $\tilde{\psi}$ always possess a parity opposite to that of $\tilde{a}_{\lambda\nu}$ and $\tilde{b}_{\lambda\nu}$. For $d = 0$, a further subdivision is possible in that both classes of disturbances defined so far separate into those disturbances $\tilde{\phi}$, $\tilde{\theta}$ that are symmetric functions of y and those that are antisymmetric in y. In table 1 the respective instabilities are described by S and A. The instabilities which correspond to finite values of d are denoted by D. The symmetry of the function $\tilde{\psi}$ is, of course, opposite again to that of $\tilde{\phi}$ and $\tilde{\theta}$.

In table 1 all instabilities are listed that have been found in the case of convection rolls with rigid top and bottom boundaries. The two new blob instabilities described in this paper have been included. Sometimes two different names are used when the instability corresponds to a long section of the stability boundary in the (R, α)-plane and when its properties vary accordingly. But usually the different instabilities are well defined and well separated in the space of their parameters.

The cross-roll and zigzag instabilities have already been mentioned by Schlüter, Lortz & Busse (1965). They have been studied in more detail by Busse (1967, 1971) and observed experimentally by Busse & Whitehead (1971). The Eckhaus instability (Busse 1971) represents a purely two-dimensional mechanism restricting the range of stable wavenumbers α to around the critical value α_c. The even-oscillatory instability was observed experimentally by Willis & Deardorff (1970) and has been described theoretically by Busse (1972). First computations in the presence of rigid boundaries have been reported in I. The skewed-varicose instability has been discussed both from the theoretical and experimental point of view by Busse & Clever (1979). Additional data can be found in Clever & Busse (1978).

In this paper further information will be provided for all instabilities mentioned above; but attention will be focused on two new oscillatory instabilities, BO2 and BE1, which feature circulating blobs of fluid with a temperature deviating from the equilibrium value. Even though only a small fraction of the stability boundary corresponds to these instabilities, the mechanism appears to be realized in a large part of the parameter space of convection at high Rayleigh numbers.

4. Stability Boundaries at $P = 2.5$ and $P = 4.0$

Since laboratory convection experiments are usually done at a nearly constant Prandtl number, plots of the stability boundaries for a given value of P provide the most useful information about the results of the stability analysis. In recent years the range $2 \lesssim P \lesssim 5$ has become of considerable interest because experiments on convection in hot water fall within this range. In figure 1 the stability boundaries are displayed for $P = 2.5$, which corresponds to a water temperature of about 70 °C. Comparison of figure 1 with the stability boundaries for $P = 0.71$ shown in I indicates that the region of stable rolls is extended greatly towards higher Rayleigh numbers

Instability	*y*-symmetry	*R*-symmetry	$\lvert d_m \rvert$	$\lvert b_m \rvert$	σ_i	P-range	α-range
Cross-roll	*S*	odd	0	$\gtrsim \alpha_c$	0	$1.1 \lesssim P$	$\gtrsim \alpha_c$
Knot	*S*	odd	0	$\lesssim \alpha_c$	0	$1.1 \lesssim P \lesssim 10$	$\gtrsim \alpha_c$
BO2	*S*	odd	0	≈ 3.1	$\sim 2\Omega^*$	$2 \lesssim P \lesssim 8$	$< \alpha_c$
BE1	*S*	even	0	≈ 4	$\sim \Omega^*$	$7 \lesssim P \lesssim 12$	$< \alpha_c$
Zigzag	*A*	even	0	> 0	0	$2 \lesssim P$	$< \alpha_c$
E-oscillatory	*A*	even	0	≈ 2	$\sim \Omega^*$	$P \lesssim 2.5$	$\lesssim \alpha_c$
Eckhaus	*D*	even	$\ll 1$	0	0	$P \lesssim 1$	$\lesssim \alpha_c$
Skewed-varicose	*D*	even	$\ll 1$	$\ll 1$	0	$P \lesssim 30$	$\lesssim \alpha_c$

TABLE 1. Instabilities of convection rolls in the presence of rigid boundaries. $2\pi/\Omega^*$ corresponds to the circulation period in the convection roll

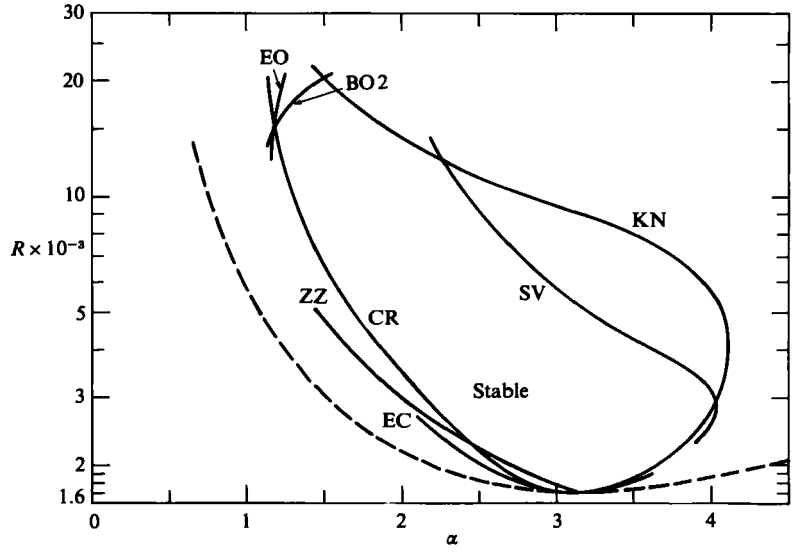

FIGURE 1. Stability boundaries of convection rolls for $P = 2.5$ as a function of the Rayleigh number R and the wavenumber α. The boundaries correspond to the cross-roll (CR), knot (KN), skewed-varicose (SV), Eckhaus (EC), zigzag (ZZ), even oscillatory (EO) and BO2 instabilities. The dashed line indicates the Rayleigh number for onset of convection.

and slightly towards lower wavenumbers but is otherwise changed relatively little in its shape. The main exception is the replacement of the even oscillatory instability by a new oscillatory instability which is denoted by BO2 in table 1. This replacement happens relatively quickly as a function of Prandtl number. It starts at about $P = 2.2$ and has just been completed at $P = 2.5$, as can be seen from the information contained in figures 1 and 6.

Figure 2 shows that the two-blob instability BO2 is characterized by two fluid parcels slightly hotter and two fluid parcels slightly colder than the long-time average, circulating around in the convection roll. During the vertical movement the blobs of neighbouring rolls join. Once they have arrived at the opposite boundary they separate again. During the horizontal motion the upper and lower blobs remain quite distinct because they move in opposite directions and less time is available for

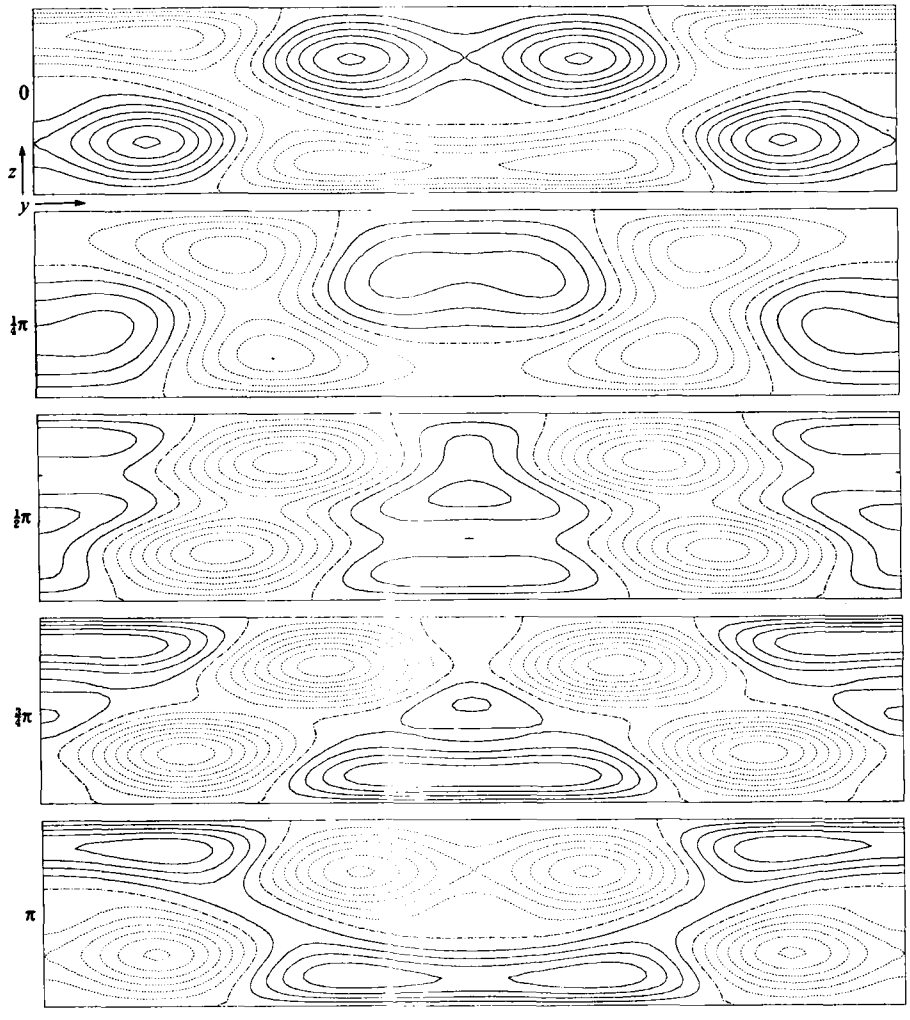

FIGURE 2. The disturbance of temperature field of the BO2 instability in the plane $x = 0$ for a sequence of phases, $\sigma_i t = 0, \frac{1}{4}\pi, \frac{1}{2}\pi, \frac{3}{4}\pi$. Positive and negative values of $\tilde{\theta}(y, z)$ correspond to solid and dashed lines respectively.

the diffusive coalescence of their temperature fields. The blobs are limited in their transverse scale along the roll axis. The value of the wavenumber b at which the growth rate reaches a maximum is around 3.5, according to figure 3. In this figure real and imaginary parts of σ are drawn for both the even oscillatory instability and the two-blob instability BO2. The period $2\pi/\sigma_i$ of the two-blob instability corresponds to one half of the circulation time in a convection roll and thus decreases as the Rayleigh number increases but is nearly independent of b. The period of the even-oscillatory instability also scales with the circulation time but exhibits a strong dependence on b. In fact, the oscillatory instability ceases to exist for small values of b. As shown in figure 3, the two complex-conjugate eigenvalues σ approach the real axis around $b = 0.45$ and separate into two real eigenvalues, one becoming the eigenvalue $\sigma = 0$ at $b = 0$, which corresponds to a translation of the roll pattern in the x-direction. This behaviour is different from that of the even-oscillatory instability

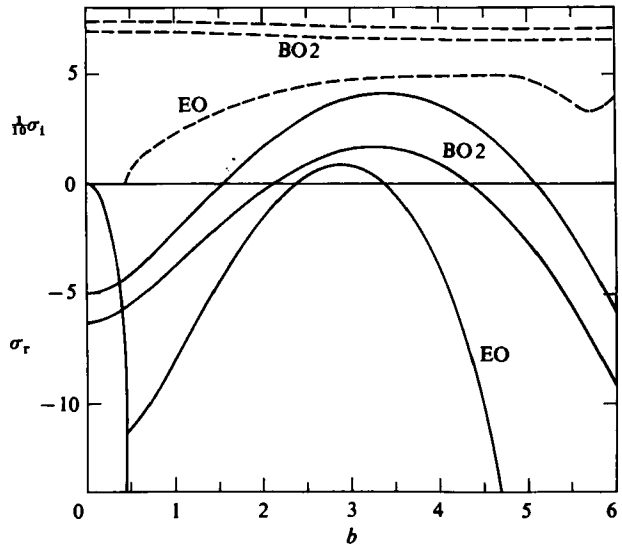

FIGURE 3. The real (solid lines) and imaginary (dashed lines) parts of the growth rate σ for the even oscillatory ($P = 2.5$, $\alpha = 1.2$, $P = 19000$) and for the BO2 ($R = 18000$ and 20000, $P = 2.5$, $\alpha = 1.25$) instabilities.

in the case of stress-free boundaries, in which case the instability occurs in the limit of small values of b (Busse 1972). For this reason the vanishing of the imaginary part σ_i at a small, but finite, value of b was overlooked in I, where a coarser grid of b-values had been used. An impression of the horizontal time-dependent pattern introduced by the two-blob BO2 instability can be gained from figure 4. In contrast to figure 2, which shows only the disturbance temperature field $\tilde{\theta}$, the total isotherms, $\theta + \epsilon\tilde{\theta} =$ constant, have been plotted in figure 4. The small-value ϵ is arbitrarily chosen in order to indicate the deviations from the two-dimensional steady isotherms introduced by the instability. As can be seen from figures 2 and 4, the blob features of the instability are most pronounced near the boundaries, in particular near the stagnation points where the upward and downward flows meet the cold and hot boundaries respectively. This property indicates that the thermal signature of the instability is roughly proportional to the gradient of the temperature field of the convection rolls. A periodic thinning and thickening of the thermal boundary layers associated with an acceleration and deceleration of the up- and down-moving flow appears to be the basic ingredient of the instability. This property is also suggested by the dominance of the $\tilde{a}_{\pm 12}$ coefficients of the disturbance eigenvector.

Relatively little change is exhibited by the stability boundaries when the Prandtl number is changed from 2.5 to 4.0. Only a small part of the stability region is shown in figure 5, where the results for the two Prandtl numbers are compared. The even-oscillatory instability is strongly affected by the increase of the Prandtl number and so has not been included in the figure for $P = 4.0$. On the other hand, a third oscillatory instability becomes noticeable, the one-blob instability BE1, which eventually replaces the two-blob instability as the Prandtl number is further increased. The truncation parameter $N = 8$ has been used for most of the computations reported in this paper. In figure 5 results are also shown for $N = 10$ in the case $P = 4.0$. The difference between the two curves provides a measure for the uncertainty of the stability boundary.

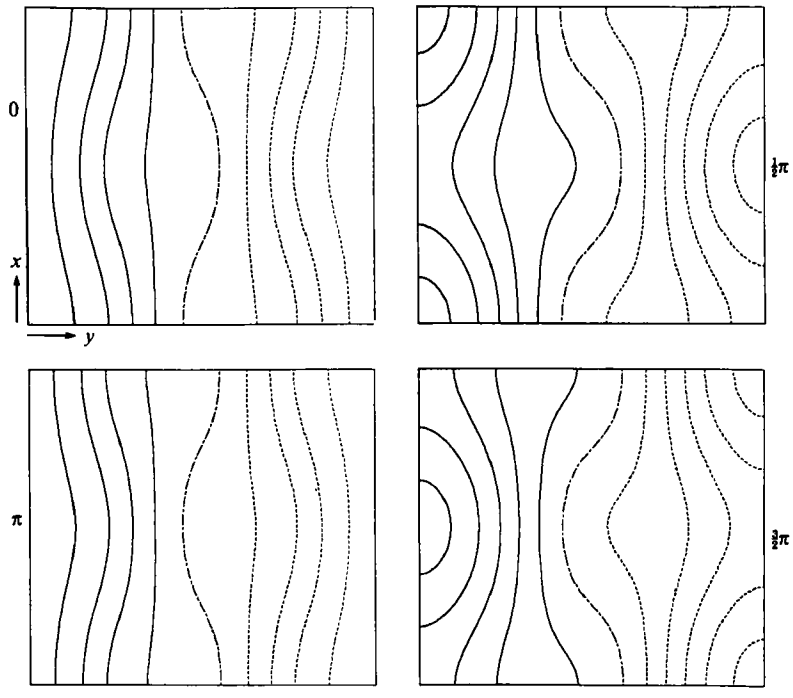

FIGURE 4. The isotherms in the midplane $z = 0$ of the BO2 instability superimposed onto the steady-roll solution. The disturbance eigenvector has been normalized such that $\tilde{a}_{01} = 0.4$. The four graphs show the isotherms at the times $\sigma_1 t = 0, \frac{1}{2}\pi, \pi, \frac{3}{2}\pi$.

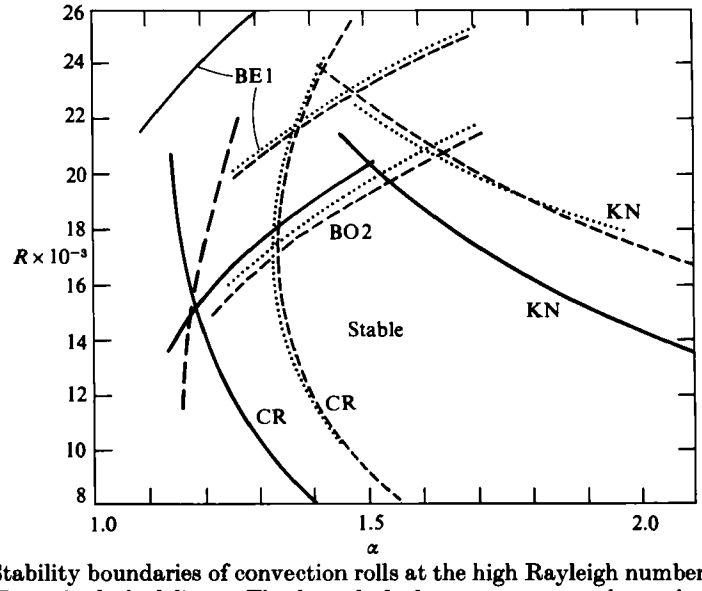

FIGURE 5. Stability boundaries of convection rolls at the high Rayleigh numbers for $P = 2.5$ (solid lines) and $P = 4.0$ (dashed lines). The long-dashed curve corresponds to the onset of the even oscillatory instability. The dotted lines indicate the stability boundaries for $P = 4.0$ corresponding to the truncation parameter $N = 10$ instead of $N = 8$.

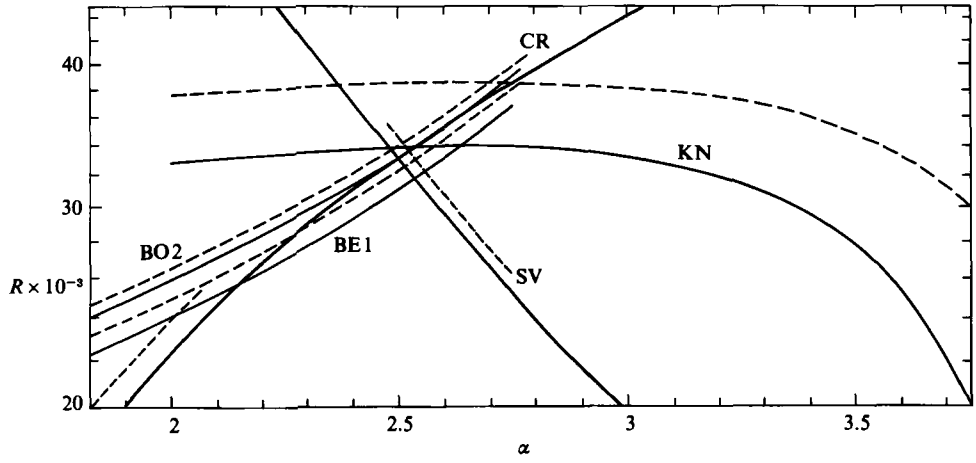

FIGURE 6. Upper part of the stability boundaries of rolls for $P = 10$. The dashed lines correspond to growth rates $\sigma = 1$. The notation is the same as in figure 1.

5. Stability boundaries for P greater than 7

Because the stability boundary corresponding to the onset of the cross-roll instability moves towards larger values of α with increasing Prandtl number, the length of the boundary of the domain of the stable rolls corresponding to the onset of the BO2 instability decreases. At $P = 7$ only a tiny triangle at the top of the stability domain is cut off by this instability. Except for this tiny triangle the stability region for $P = 7$ shown in I is unchanged. The Prandtl number 7 also marks the first time at which with increasing P the onset of the one-blob instability BE1 becomes part of the stability boundary. In particular the stability boundaries of the two oscillating blob instabilities, BE1 and BO2, cross at a small angle at about $\alpha = 2.0$, $R = 26 \times 10^3$ for $P = 7$. Because the upper intersection between cross-roll- and knot-instability boundaries moves towards higher Rayleigh numbers for $P \gtrsim 7$, the section of the stability boundary corresponding to the onset of the BE1 instability increases when the Prandtl number is increased beyond $P = 7$. Figure 6 shows the section of the stability region of interest for $P = 10$. This figure also includes lines at which the maximum growth rates of the instabilities reach 1.0 in dimensionless units. These lines thus give an indication of the strength of growth of the respective instabilities once the stability boundaries have been passed.

Figure 7 gives an impression of the spatial structure and time dependence of the BE1 instability. Except for the basic difference that only one hot and one cold blob are circulating, the instability closely resembles the BO2 instability. The imaginary part σ_i of the growth rate is again independent of b and is approximately half as large as the corresponding value of the BO2 instability. The values of b maximizing the growth rate lie in the neighbourhood of 4.5 in the region where the instability forms the stability boundary. They tend to increase with Prandtl number. Figure 8 gives an impression of the horizontal structure by indicating the isotherms of the combined roll-plus-disturbance solution, $\theta + \epsilon\tilde{\theta}$, where a suitable value of ϵ has been chosen. The main difference that can be seen in the comparison with figures 2 and 4 is the preservation of the symmetry of the basic rolls in the (y, z)-plane by the BE1 instability.

The BE1 instability resembles closely the oscillatory instability found by Kessler, Dallman & Oertel (1984) in independent computations of convection in a horizontal

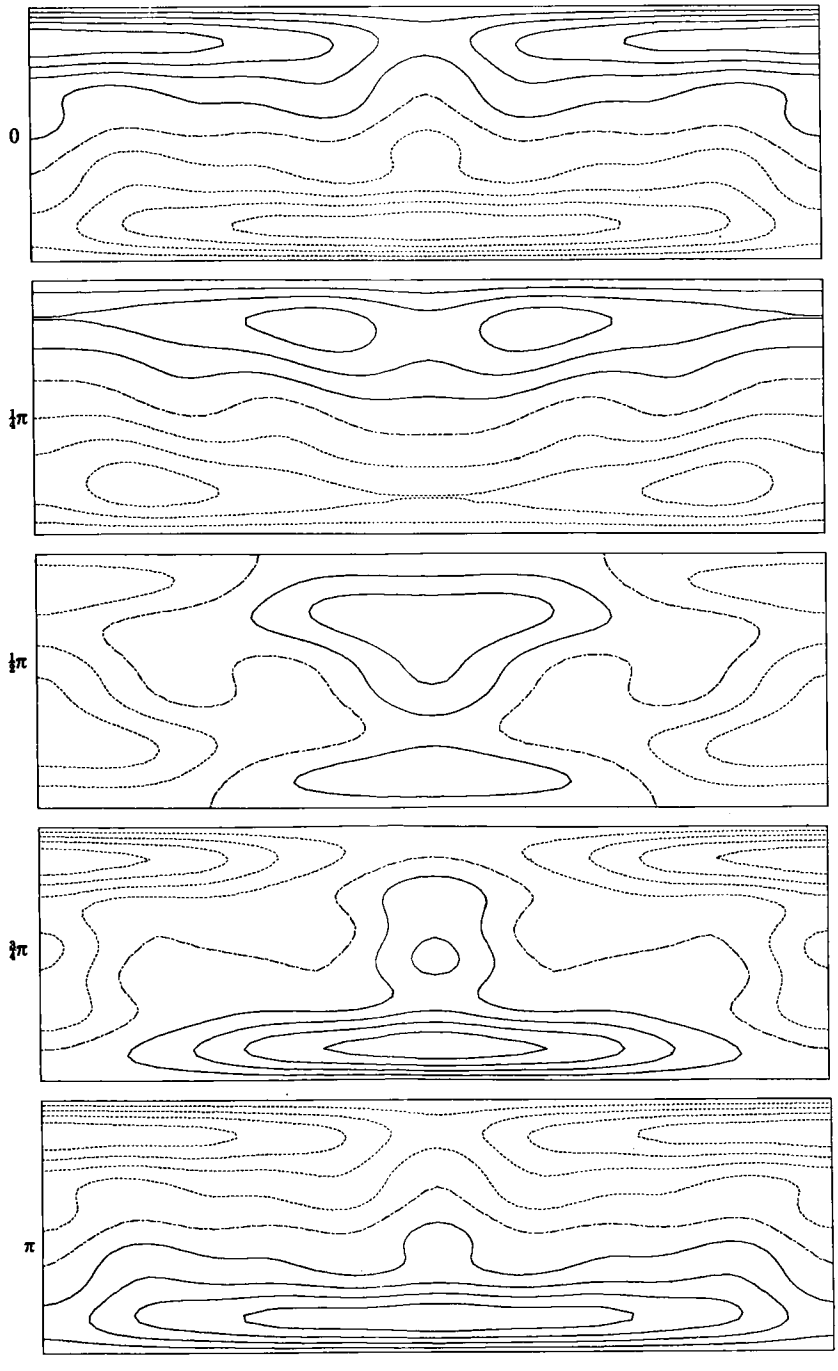

FIGURE 7. The disturbance temperature field in the plane $x = 0$ for different phases of the BE1 instability. Positive and negative values of $\tilde{\theta}(y, z)$ correspond to solid and dashed lines respectively.

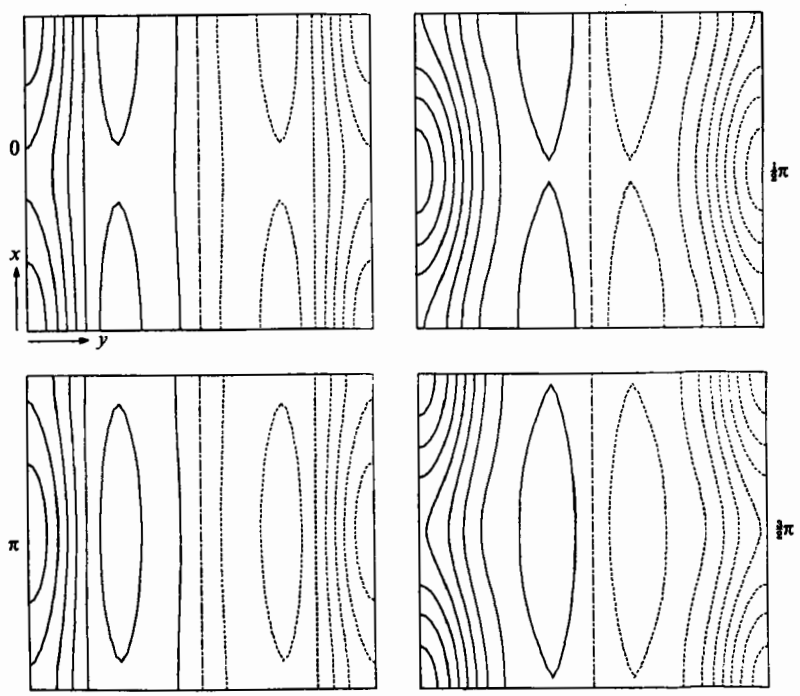

FIGURE 8. The isotherms in the midplane $z = 0$ of the BE1 instability superimposed on the steady-roll solution. The disturbance eigenvector has been normalized such that $\tilde{a}_{02} = 0.3$. The four graphs show the isotherms at the times $\sigma_i t = 0, \frac{1}{2}\pi, \pi, \frac{3}{2}\pi$.

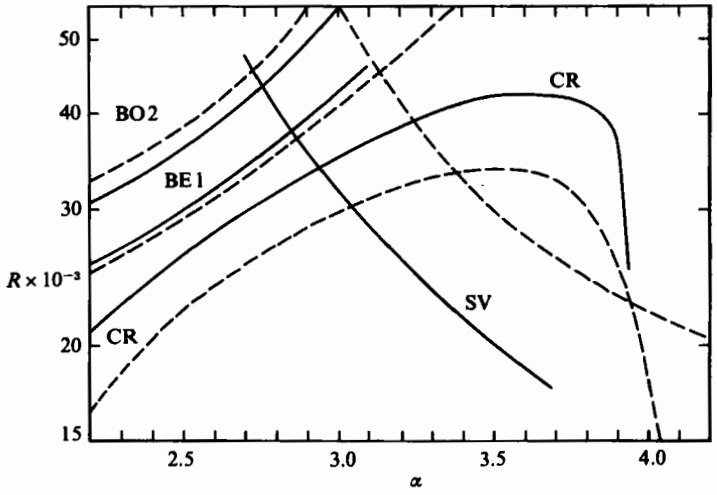

FIGURE 9. Stability boundaries of rolls for $P = 16$ (solid) and $P = 25$ (dashed). Notation is the same as in earlier figures.

box of finite size for $P = 7$. At the high Rayleigh numbers, of order 7×10^4, used by these authors the transition to a bimodal pattern of convection must be expected to have occurred. But this transition could not be realized in the computations because of the limited numerical resolution in the direction parallel to the roll axis.

Although the BE1 instability is nearly independent of the Rayleigh number for $P \gtrsim 3$, it does not correspond to a part of the boundary of the domain of stable rolls

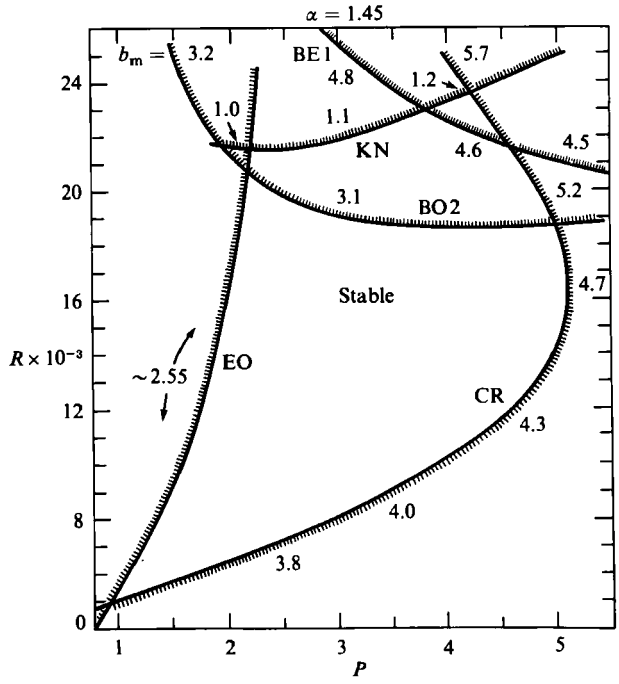

FIGURE 10. Cross-section of the domain of stable rolls in the (R, P, α)-space for constant $\alpha = 1.45$. Notation is the same as in figure 1. The numbers at the curves refer to the maximizing values b_m.

for $P \gtrsim 12$ because the cross-roll stability boundary moves towards somewhat lower Rayleigh number as P increases. That the onset of BE1 instability becomes independent of P has been checked by computations for $P = 10^3$. Using a wavenumber $\alpha = 3.0$ we find that the onset of the BE1 instability drops from $R = 42 \times 10^3$ to $R = 38 \times 10^3$ when P is changed from 25 to 10^3. The imaginary part σ_i changes from 136 to 128 and the maximizing value of b stays at about the same value of 5.2.

Figure 9 shows the stability boundaries for both $P = 16$ and 25. The stability boundary for the knot instability has merged with that of the cross-roll boundary as will be discussed in more detail in the next section. The skewed-varicose instability is still important at $P = 25$ but by extrapolation of the results shown in the figure it can be concluded that this instability will be preceded for all α by the cross-roll instability when P exceeds 30. Thus the region of stable rolls rapidly approaches the shape obtained for infinite Prandtl number (Busse 1967) and there seems to be no need to calculate stability boundaries for the range $25 \leqslant P \leqslant 100$.

6. Prandtl-number dependence of stability boundaries

Although stability boundaries of convection rolls have been discussed in the preceding sections at fairly closely spaced values of P, it is illuminating to see more directly the dependence of the instabilities on the Prandtl number. Figure 10 describes a cross-section of the stability surfaces at a constant value of α in the (R, P, α)-parameter space of steady-roll solutions. This cross-section indicates that rolls with low values of α are stable only for a limited range of Prandtl number. The lowest possible value of α for a stable roll has not been calculated; it probably lies close to 1.1. Figure 10 shows clearly the strong Prandtl-number dependence of the

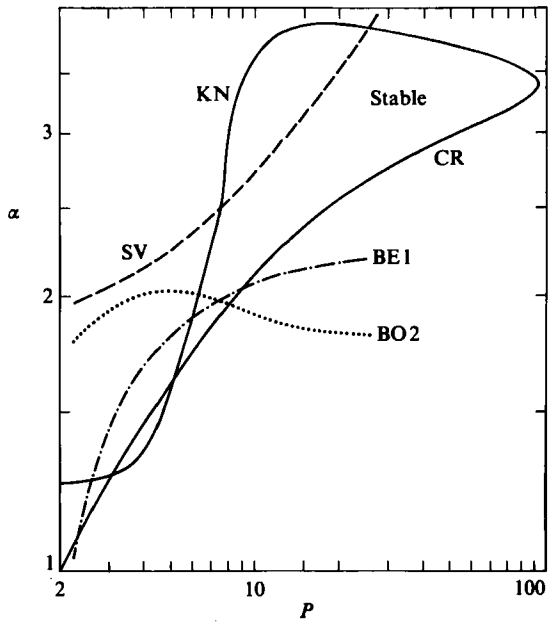

FIGURE 11. Cross-section of the domain of stable rolls in the (R, P, α)-space for constant $R = 25 \times 10^3$. Notation is the same as in figure 1.

even oscillatory instability and the much weaker dependence on P of the blob instabilities. A number of additional blob instabilities have been followed in the computations leading to this paper; but, since they were always preceded by other instabilities, they are not described here in detail. A BO4 and a BE3 instability have been found at Rayleigh numbers slightly above those required for the BO2 or the BE1 instability. As is suggested by the nomenclature, the BE3 instability differs from the BE1 instability essentially only in that three hot and three cold blobs circulate in a convection roll instead of one hot and one cold blob. This property is also evident in the frequencies σ_i associated with the instabilities. The value of σ_i for the BE3 instability agrees to within a few percent with three times the value of σ_i for the BE1 instability.

A different cross-section of the stability surfaces in the (R, P, α)-space is shown in figure 11. At the relatively high value of $R = 25 \times 10^3$ a region of stable rolls exists only for $6.3 \lesssim P \lesssim 103$. Several instabilities are involved in bounding the stability region and the structure of interacting surfaces becomes quite complex in the lower left corner of the figure. Of particular interest is the junction of the cross-roll and knot instabilities which occurs near the top of figure 11. These two instabilities are unusual in that they do not differ in their symmetry properties. They even correspond to the same eigenvalue $\sigma(b)$ as a function of the wavenumber b along the axis of the roll solution. Their main distinction is the value b_m of b maximizing the growth rate σ_r. As shown in figure 12 as a typical example for the region $P \lesssim 10$, the growth rate σ displays a typical double-humped structure as a function of b. The hump corresponding to $b_m < \alpha_c$ belongs to the knot instability while the cross-roll instability exhibits a maximizing value b_m above α_c. The two peaks of σ reach equal values at the crossing point of the two stability boundaries. But the double-hump feature is noticeable over a large region of the parameter space for $P \lesssim 10$. That the two instabilities are quite distinct for $P \lesssim 10$ while they lose their distinction for higher

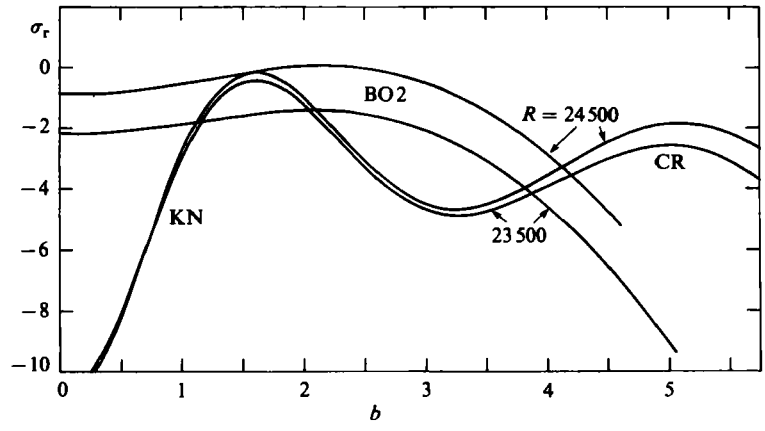

FIGURE 12. Growth rates σ_r as a function of b for the knot and cross-roll instabilities and the BO2 instability for the indicated values of the Rayleigh number R at $P = 7$ and $\alpha = 1.95$.

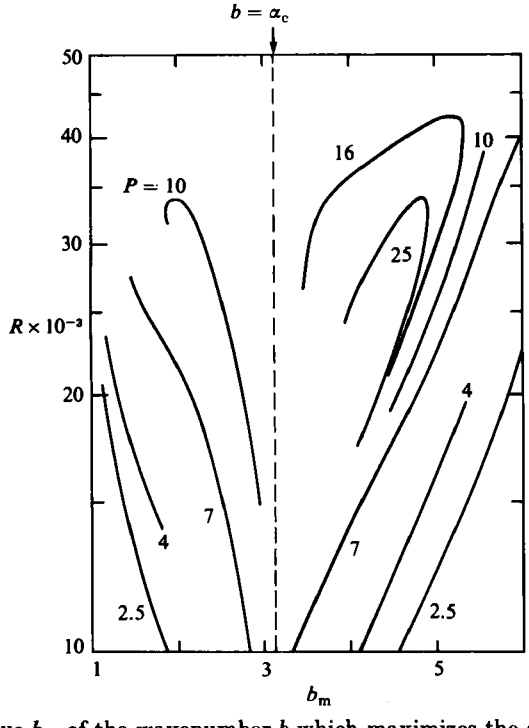

FIGURE 13. The value b_m of the wavenumber b which maximizes the growth rate at the stability boundary for the knot instability ($b_m < \alpha_c$) and for the cross-roll instability ($b_m > \alpha_c$). Numbers refer to the Prandtl numbers.

Prandtl numbers can be seen in figure 13, which depicts the maximizing values of b_m along both stability boundaries for different values of P. The separation of the two humps which characterizes the growth rate as a function of b in the neighbourhood of the crossing of the stability boundaries increases with decreasing P for $P \lesssim 10$. For $P \gtrsim 16$, however, only a single maximum of σ occurs as a function of b. Between the Prandtl numbers 10 and 16 the knot-instability peak merges within the shoulder of the cross-roll-instability peak. It thus seems reasonable to associate the entire

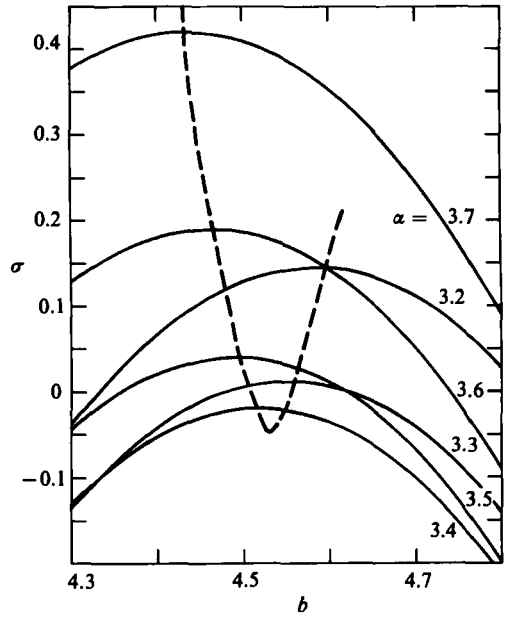

FIGURE 14. The growth rate σ of the cross-roll instability as a function of b for $R = 25 \times 10^3$, $P = 25$, and different values of α as indicated in the figure. The dashed line connects the maximizing values b_m.

stability boundary with the cross-roll instability for $P \gtrsim 16$, but to introduce the name knot instability for the instability responsible for the right branch of the stability boundary in (R, α)-diagram when P is of the order 10 or less.

As shown in figure 14, the growth rate σ of the cross-roll instability exhibits basically the same dependence on the parameter for $P \gtrsim 16$ as in the case of infinite Prandtl number (Busse 1967). In particular, there exists a certain α, between 3.3 and 3.4, where the maximum growth rate reaches a minimum for a given value of R.

7. Discussion

The new mechanisms of oscillatory blob instability discussed in this paper have not much changed the general shape of the stability domain of steady rolls in the (R, P, α)-space as it had emerged from the earlier less detailed computations (see, for example, figure 13 of Busse 1978). The new instability mechanisms are important, however, because like most of the other mechanisms of instability they continue to operate after the two-dimensional structure of steady rolls has been changed into a three-dimensional form of convection. Because of their different symmetry properties, the different mechanisms of instability interfere relatively little with each other in general. The one-blob- and two-blob-type oscillations are usually observed after the convection flow has become three-dimensional, primarily through the transition to bimodal convection. But measured dependences on the parameters R and P of the frequencies of oscillations closely resemble those extrapolated from the results described in this paper. The doubling of the frequency corresponding to the transition from one-blob to two-blob oscillations has been noticed by Rossby (1966) and Willis & Deardorff (1967), but the nature of these oscillations was first elucidated by Krishnamurti (1970). Because liquids with $P \gtrsim 10$ were mostly used in the experiments

the one-blob oscillations are predominantly seen. Another reason for the preference of the BE1 mechanism could be the high value of b_m, which makes this mechanism more compatible with the bimodal pattern of convection. An example of relatively pure one-blob oscillation can be seen in figure 9 of Busse & Whitehead (1974). At larger secondary wavelength of the bimodal cell or at lower Prandtl numbers the oscillations combine features of the even oscillatory and the one-blob instabilities as seen in their figures 6, 7 and 8.

Oscillations with numerous frequencies have also been observed in the convection experiments of Walden *et al.* (1984) and Kolodner *et al.* (1985). Because of the relatively small aspect ratio of their convection layer, the convection pattern is strongly influenced by the sidewalls and some frequencies correspond to oscillations in different parts of the convection layer. While it is thus not possible to find a clear relationship between the frequencies and the number of blobs circulating in the respective convection cell, the experiments provide very accurate measurements of the frequency spectrum and confirm the general picture that has emerged from the earlier experiments.

The observations of instabilities of convection rolls are not only affected by the degree to which the two-dimensional roll structure is realized in the experiment but also by the growth rates of the instabilities. The stability boundary extrapolated from laboratory observations may differ from the theoretical one because only instabilities with sufficiently high growth rates are seen in experiments. Among instabilities with neighbouring stability boundaries the instability with the strongest growth rate is thus most likely to be seen in the experiment and not necessarily the instability which actually bounds the domain of stable rolls. So far no significant discrepancy between theory and experimental observations has been reported. This suggests that subcritical finite-amplitude onset of instabilities does not occur. There is also no experimental indication for the onset of the oscillatory skewed-varicose instability in the presence of rigid boundaries. This instability seems to occur only in the presence of stress-free boundaries (Busse & Bolton 1984; Bolton & Busse 1985). A search for such an instability has been conducted for low values of P in the course of the present investigation. Although a local maximum of the real part of σ with associated finite imaginary part σ_i was found for values of d and b in the neighbourhood of 0.5, this maximum of σ_r always remained negative within the domain of stable rolls.

An interesting question which has not been answered by the analysis of this paper is the effect of the new instabilities on the convective heat transport. Krishnamurti's (1970) observations suggest an increase of the heat transport due to the oscillations. Since changes in the pattern of convection often occur concurrently with the onset of oscillations, it is not always clear how much oscillations contribute to the heat transport. A theoretical analysis based on a perturbation approach for small amplitudes of oscillations could eventually elucidate this problem. But such an extension of the present calculations goes beyond the scope of this paper.

The authors of this paper gratefully acknowledge the help they have received from Mr Brian Dodd and Ms Anyang Feng in carrying out some of the often tedious computations. The research has been supported by the Atmospheric Science Section of the U.S. National Science Foundation. The main results of this paper have been presented at an APS Fluid Dynamics Division meeting (Bolton, Busse & Clever 1983).

REFERENCES

AHLERS, G. & BEHRINGER, R. P. 1978 Evolution of turbulence from the Rayleigh-Bénard instability. *Phys. Rev. Lett.* **40**, 712–716.

BOLTON, E. W. & BUSSE, F. H. 1985 Stability of convection rolls in a layer with stress-free boundaries. *J. Fluid Mech.* **150**, 487–498.

BOLTON, E. W., F. H. BUSSE & R. M. CLEVER 1983 An antisymmetric oscillatory instability of convection rolls. *Bull. Am. Phys. Soc.* **28**, 1399.

BUSSE, F. H. 1967 On the stability of two-dimensional convection in a layer heated from below. *J. Math. Phys.* **46**, 140–150.

BUSSE, F. H. 1971 Stability regions of cellular fluid flow. In *Instability of Continuous Systems* (ed. H. Leipholz), pp. 41–47. Springer.

BUSSE, F. H. 1972 The oscillatory instability of convection rolls in a low Prandtl number fluid. *J. Fluid Mech.* **52**, 97–112.

BUSSE, F. H. 1978 Nonlinear properties of convection. *Rep. Prog. Phys.* **41**, 1929–1967.

BUSSE, F. H. & BOLTON, E. W. 1984 Instabilities of convection rolls with stress-free boundaries near threshold. *J. Fluid Mech.* **146**, 115–125.

BUSSE, F. H. & CLEVER, R. M. 1979 Instabilities of convection rolls in a fluid of moderate Prandtl number. *J. Fluid Mech.* **91**, 319–335.

BUSSE, F. H. & WHITEHEAD, J. A. 1971 Instabilities of convection rolls in a high Prandtl number fluid. *J. Fluid Mech.* **47**, 305–320.

BUSSE, F. H. & WHITEHEAD, J. A. 1974 Oscillatory and collective instabilities in large Prandtl number convection. *J. Fluid Mech.* **66**, 67–79.

CLEVER, R. M. & BUSSE, F. H. 1974 Transition to time-dependent convection. *J. Fluid Mech.* **65**, 625–645.

CLEVER, R. M. & BUSSE, F. H. 1978 Large wave length convection rolls in low Prandtl number fluids. *Z. angew. Math. Phys.* **29**, 711–714.

FAUVE, S., LAROCHE, C. & LIBCHABER, A. 1981 Effect of a horizontal magnetic field on convection instabilities in mercury. *J. Physique Lett.* **42**, L455–L457.

GOLLUB, J. P. & BENSON, S. V. 1980 Many routes to turbulent convection. *J. Fluid Mech.* **100**, 449–470.

GOLLUB, J. P. & STEINMAN, J. F. 1981 Doppler imaging of the onset of turbulent convection. *Phys. Rev. Lett.* **47**, 505–508.

KESSLER, R., DALLMANN, V. & OERTEL, H. 1984 Nonlinear transitions in Rayleigh–Bénard convection. In *Turbulence and Chaotic Phenomena in Fluids* (ed. T. Tatsumi), pp. 173–178. Elsevier.

KRISHNAMURTI, R. 1970 On the transition to turbulent convection. Part 2. The transition to time-dependent flow. *J. Fluid Mech.* **42**, 309–320.

KOLODNER, P., WALDEN, R. W., PASSNER, A. & SURKO, C. M. 1985 Stability of Rayleigh–Bénard convection patterns in a rectangular container. *Preprint.*

ROSSBY, H. T. 1966 An experimental study of Bénard convection with and without rotation. Ph.D. thesis, Massachusetts Institute of Technology.

SCHLÜTER, A., LORTZ, D. & BUSSE, F. 1965 On the stability of steady finite amplitude convection. *J. Fluid Mech.* **23**, 129–144.

WALDEN, R. W., KOLODNER, P., PASSNER, A. & SURKO, C. M. 1984 Nonchaotic Rayleigh–Bénard convection with four and five incommensurate frequencies. *Phys. Rev. Letts.* **53**, 242–245.

WILLIS, G. E. & DEARDORFF, J. W. 1967 Development of short-period temperature fluctuations in thermal convection. *Phys. Fluids* **10**, 931–937.

WILLIS, G. E. & DEARDORFF, J. W. 1970 The oscillatory motions of Rayleigh convection. *J. Fluid Mech.* **44**, 661–672.